POLITECNICO DI TORINO
Repository ISTITUZIONALE

Coupled chemical-hydraulic-mechanical behaviour of bentonites

Original
Coupled chemical-hydraulic-mechanical behaviour of bentonites / Dominijanni, A., Manassero, M., Puma, S.. - In: GEOTECHNIQUE. - ISSN 0016-8505. - STAMPA. - 63:3(2013), pp. 191-205. [10.1680/geot.SIP13.P.010]

Availability:
This version is available at: 11583/2502007 since:

Publisher:
ICE PUBLISHING

Published
DOI:10.1680/geot.SIP13.P.010

Terms of use:

This article is made available under terms and conditions as specified in the corresponding bibliographic description in the repository

Publisher copyright
SPIIE [DA NON USARE]

Da definire

(Article begins on next page)

12 September 2026

Dominijanni, A. *et al.* (2013). *Géotechnique* **63**, No. 3, 191–205 [http://dx.doi.org/10.1680/geot.SIP13.P.010]

Coupled chemical-hydraulic-mechanical behaviour of bentonites

A. DOMINIJANNI*, M. MANASSERO* and S. PUMA*

Bentonites are clay soils characterised by a high specific surface and a permanent negative electric charge on their solid skeleton. Their common use as hydraulic and contaminant barriers for landfill and soil remediation applications, including the final disposal of nuclear waste, needs to be supported by adequate theoretical modelling of their mechanical behaviour and transport properties, in order to assess the expected performance in the long term. To this end, a theoretical approach has been proposed in order to derive constitutive equations for their coupled chemical-hydraulic-mechanical behaviour. The phenomenological parameters that govern the transport of electrolyte solutions through bentonites – that is, the hydraulic conductivity, the reflection coefficient (which is also called the chemico-osmotic efficiency coefficient), and the osmotic effective diffusion coefficient – have been measured through laboratory tests on a bentonite with porosity of 0·81, over a range of sodium chloride concentrations in the pore solution that varied from 5 mM to 100 mM. The relevance of the osmotic phenomena has been shown to decrease when the salt concentration increases. The obtained results have been interpreted by assuming that the microscopic deviations of the pore solution state variables from their average values are negligible. In this way, it is possible to interpret the macroscopic behaviour on the basis of the physical and chemical properties of the bentonite mineralogical components.

KEYWORDS: chemical properties; clays; constitutive relations; expansive soils; laboratory tests; pore pressures

INTRODUCTION

The term 'bentonite' is commonly used to indicate a clay soil with a high content ($> 70\%$) of montmorillonite, a mineral of the smectite group. Montmorillonite particles are thin lamellae that are characterised by a high specific surface (defined as the surface per unit weight) and a permanent negative electric charge. Bentonite is used in hydraulic and contaminant barriers, because of its low hydraulic conductivity, k, to permeation with water and dilute aqueous solutions (k typically $\leqslant 3 \times 10^{-11}$ m/s). Geosynthetic clay liners (GCLs), which consist of a thin layer of bentonite (~5–10 mm thick) sandwiched between two geotextiles, are examples of such barriers. GCLs are currently used in bottom and cover landfill barriers to limit water infiltration and contaminant migration.

Owing to its physical and chemical properties, bentonite's macroscopic mechanical behaviour and transport properties cannot be modelled through classical soil mechanics approaches (Manassero & Dominijanni, 2003). In fact, bentonite swells or shrinks in response to changes in the chemical composition of the pore solution. Moreover, when a hydraulic pressure gradient, or a solute concentration gradient, is applied to it, both a volumetric flux and a diffusive solute mass flux occur, as in semi-permeable membranes. For this reason, a theoretical approach that accounts for the electric interaction that occurs between the solid skeleton of the bentonite and the ions contained in the pore solution is proposed in the first part of this paper. The experimental determination of the swelling pressure and the transport properties of a natural sodium bentonite is described in the second part. The obtained results have been interpreted with the proposed theoretical model, in which the microscopic properties of the bentonite have been linked to the observed macroscopic behaviour.

Manuscript received 29 February 2012; revised manuscript accepted 22 October 2012.
Discussion on this paper closes on 1 August 2013, for further details see p. ii.
* Department of Structural, Geotechnical and Building Engineering, Politecnico di Torino, Torino, Italy.

THEORY

Montmorillonite lamellae are characterised by a negative electric charge, owing to the isomorphic substitution of a portion of the tetravalent silicon (Si^{4+}) and the trivalent aluminium (Al^{3+}) in their crystalline structure, with metals, such as magnesium (Mg^{2+}), which have a lower valence. This electric charge per unit solid volume can be expressed as $F \cdot \bar{c}_{sk,0}$, where F is Faraday's constant (96 485 C/mol) and $\bar{c}_{sk,0}$ is the molar concentration per unit solid volume of the solid skeleton electric charge, which is assumed to have unit valence (i.e. $z_{sk} = -1$). $\bar{c}_{sk,0}$ represents the moles of solid skeleton electric charge per volume of solids and, in order to be compared with the ion concentrations of the pore solution, it needs to be divided by the void ratio, e, which represents the pore volume per volume of solids. Dominijanni & Manassero (2012b) have shown that $\bar{c}_{sk,0}$ is proportional to the effective specific surface of the solid particles, and decreases when the montmorillonite lamellae aggregate to form the so-called *tactoids*.

If the pore solution contains a single salt that is completely dissociated with the stoichiometric reaction

$$(\text{Cation})_{z_1}^{\nu_1}(\text{Anion})_{z_2}^{\nu_2} \rightarrow \nu_1(\text{Cation})^{z_1} + \nu_2(\text{Anion})^{z_2}$$

where z_1 and z_2 are the electrochemical valences of the cation and the anion, and ν_1 and ν_2 are the stoichiometric coefficients of the cation and the anion respectively, then the following condition has to be satisfied in order to preserve electroneutrality within a saturated porous medium, even in the presence of the solid skeleton electric charge

$$z_1\bar{c}_1 + z_2\bar{c}_2 = \frac{\bar{c}_{sk,0}}{e} \quad (1)$$

where $\bar{c}_1$ and $\bar{c}_2$ are the molar concentrations of the cation and the anion respectively, and e is the void ratio.

As a consequence, the solid skeleton electric charge influences the distribution of the ions contained in the pore solution. This phenomenon is known as the *ion partition effect*, and is expected to be more relevant for porous media characterised by higher solid skeleton charge concentrations.

Equilibrium conditions

When an electrically charged porous medium is placed in contact with an external bulk solution that contains the same ions as are present in the pore solution, a thermodynamic equilibrium condition is reached, after a certain period of time, in which the water chemical potential and the ion electrochemical potentials between the two solutions are equal. The external bulk solution can be considered as a 'chemical thermometer' in order to evaluate the equilibrium conditions of the porous medium (Coussy, 2004). The electroneutrality condition in the external solution is given by

$$z_1 c_1 + z_2 c_2 = 0 \tag{2}$$

where c_1 and c_2 are the molar concentrations of the cation and the anion that are contained in the bulk solution.

It is convenient to define the salt concentration, c_s, of the external solution as

$$c_s = \frac{c_1}{\nu_1} = \frac{c_2}{\nu_2} \tag{3}$$

Using equation (3), the electroneutrality condition, equation (2), provides the relation between the electrochemical valences and the stoichiometric coefficients as

$$z_1 \nu_1 + z_2 \nu_2 = 0 \tag{4}$$

As a result, the equilibrium condition can be characterised by the following state variables of the external bulk solution: the absolute temperature, T; the hydraulic pressure (referenced to the atmospheric pressure, as is usual in soil mechanics), u; and the salt concentration, c_s. The corresponding variables of the pore solution can be evaluated from the following conditions

$$\bar{T} = T \tag{5}$$

$$\bar{\mu}_w = \mu_w \tag{6}$$

$$\bar{\mu}_i^{ec} = \mu_i^{ec} \quad i = 1, 2 \tag{7}$$

where $\bar{T}$ and T are the absolute temperature in the pore solution and in the external bulk solution respectively; $\bar{\mu}_w$ and μ_w are the water chemical potential in the pore solution and in the external bulk solution respectively; and $\bar{\mu}_i^{ec}$ and μ_i^{ec} are the electrochemical potentials of the ith ion in the pore solution and in the external bulk solution respectively.

The water chemical potential, μ_w, and the ion electrochemical potentials, μ_i^{ec}, of the external solution can be related to the hydraulic pressure, u, and the salt concentration, c_s, for a dilute solution according to (Katchalsky & Curran, 1965; Dominijanni & Manassero, 2012a)

$$\mu_w = \mu_w^0(T) + \frac{u - \Pi}{c_w} \tag{8}$$

$$\mu_i^{ec} = \mu_i + z_i F \phi = \mu_i^0(T) + RT \ln(\nu_i c_s) + z_i F \phi \quad i = 1, 2 \tag{9}$$

where μ_w^0 and μ_i^0 are integration constants that only depend on the absolute temperature T; c_w is the water molar concentration; $\Pi = RT \sum_{i=1}^{2} \nu_i c_s$ is the osmotic pressure; μ_i is the chemical potential of the ith ion; R is the universal gas constant ($= 8{\cdot}314$ J/(mol K)); and ϕ is the electric potential.

The state variables in the external bulk solution can be measured easily, whereas it is very difficult to determine the corresponding variables in the pore solution. Moreover, the relations obtained by linking the chemical potentials to the state variables of the pore solution are more uncertain, owing to the interaction with the solid skeleton charge, which alters the ion concentration distribution near the solid particles. The simplest assumption that can be adopted involves using relations analogous to equations (8) and (9), as they are also considered valid for the pore solution. This assumption, which was first proposed by Donnan (1911), neglects the microscopic deviations of the ion concentrations from their average values that are induced by the electric potential distribution within the pores. If this approximation is accepted, then the water chemical potential, $\bar{\mu}_w$, and the ion electrochemical potentials, $\bar{\mu}_i^{ec}$, of the pore solution can be expressed as

$$\bar{\mu}_w = \bar{\mu}_w^0(T) + \frac{\bar{u} - \bar{\Pi}}{\bar{c}_w} \tag{10}$$

$$\bar{\mu}_i^{ec} = \bar{\mu}_i + z_i F \bar{\phi} = \bar{\mu}_i^0(T) + RT \ln(\bar{c}_i) + z_i F \bar{\phi} \quad i = 1, 2 \tag{11}$$

where $\bar{\mu}_w^0$ and $\bar{\mu}_i^0$ are integration constants that depend only on the absolute temperature, T; $\bar{c}_w$ is the molar concentration of the water in the pore solution, which can be taken equal to the molar concentration of the water in the external bulk solution, that is, $\bar{c}_w \cong c_w$; $\bar{\Pi} = RT \sum_{i=1}^{2} \bar{c}_i$ is the osmotic pressure of the pore solution; $\bar{\mu}_i$ is the chemical potential of the ith ion in the pore solution; and $\bar{\phi}$ is the electric potential in the pore solution.

The hydraulic pressure of the pore solution, $\bar{u}$, and the ion partition factor, Γ_i, defined as the ratio between the ion concentration of the pore solution and the ion concentration of the external bulk solution, can therefore be expressed on the basis of equations (6) and (7), and using equations (8)–(11)

$$\bar{u} = u + (\bar{\Pi} - \Pi) \tag{12}$$

$$\Gamma_i = \frac{\bar{c}_i}{c_i} = \frac{\bar{c}_i}{\nu_i c_s} = \exp\left(-z_i \frac{F}{RT} \bar{\psi}\right) \quad i = 1, 2 \tag{13}$$

where $\bar{\psi} = \bar{\phi} - \phi$ is the electric potential of the porous medium, which is also called Donnan's potential.

On the basis of this approach, the hydraulic pressure of the pore solution is different from the hydraulic pressure of the external solution that is in equilibrium with it. The pressure difference between the pore solution and the external solution is called the swelling pressure, u_{sw}, and is given by

$$u_{sw} = \bar{\Pi} - \Pi \tag{14}$$

Equations (12) and (13) for $i = 1, 2$, together with equation (1), constitute a set of four equations that can be solved to find the four unknown variables: the hydraulic pressure, $\bar{u}$, the ion concentrations, $\bar{c}_i$ for $i = 1, 2$, and the electric potential, $\bar{\psi}$.

When the ion electrochemical valences are both unitary, such as for soidium chloride, equation (13) implies that

$$\Gamma_1 = \Gamma_2^{-1} \tag{15}$$

Inserting equation (15) into equation (1) results in the equation

$$\Gamma_2^{-1} - \Gamma_2 - \frac{\bar{c}_{sk,0}}{e c_s} = 0 \tag{16}$$

which has a positive solution of the form

$$\Gamma_2 = -\frac{\bar{c}_{sk,0}}{2ec_s} + \sqrt{\left(\frac{\bar{c}_{sk,0}}{2ec_s}\right)^2 + 1} \tag{17}$$

and

$$\Gamma_1 = \Gamma_2^{-1} = \frac{\bar{c}_{sk,0}}{2ec_s} + \sqrt{\left(\frac{\bar{c}_{sk,0}}{2ec_s}\right)^2 + 1} \tag{18}$$

On the basis of equations (17) and (18), the swelling pressure can be expressed as

$$\begin{aligned} u_{sw} &= RTc_s(\Gamma_1 + \Gamma_2 - 2) \\ &= 2RTc_s\left[\sqrt{\left(\frac{\bar{c}_{sk,0}}{2ec_s}\right)^2 + 1} - 1\right] \end{aligned} \tag{19}$$

Change in equilibrium

When the hydraulic pressure and/or the salt concentration are changed in the external bulk solution, a new equilibrium condition is restored in the porous medium after a sufficiently long period of time. In order to evaluate this new condition, the change in the free energy per unit initial (undeformed) volume of the porous medium, $\Im_V$, can be determined by assuming that it is a function of the macroscopic strain tensor, $\boldsymbol{\varepsilon}$, and the concentration of each fluid component (Dormieux *et al.*, 2003). A second assumption that can be made refers to the reversible mechanical behaviour of the solid constituents: in such a case, the intrinsic dissipation, due to the solid skeleton strains, is zero (Dormieux *et al.*, 2003; Dominijanni & Manassero, 2012a). On the basis of these assumptions, the increment in free energy per unit initial volume, under isothermal conditions, can be expressed as

$$d\Im_V = \boldsymbol{\sigma} : d\boldsymbol{\varepsilon} + \sum_{k=w,1}^{2} \bar{\mu}_k \frac{d(e\bar{c}_k)}{1+e_0} \tag{20}$$

where $\boldsymbol{\sigma}$ is the total stress tensor and e_0 is the initial void ratio.

In equation (20), the chemical potentials of the pore solution, $\bar{\mu}_i$, can be substituted by the electrochemical potentials, $\bar{\mu}_i^{ec}$, since the adding term given by

$$F\bar{\phi}\left\{\frac{d[e(z_1\bar{c}_1 + z_2\bar{c}_2)]}{1+e_0}\right\} = F\bar{\phi}\frac{d\bar{c}_{sk,0}}{1+e_0}$$

is null, if the solid skeleton charge, $\bar{c}_{sk,0}$, is assumed constant.

Then, applying equations (6) and (7), the water chemical potential and the ion electrochemical potentials in the pore solution can be substituted by the corresponding potentials in the external solution. If the electroneutrality condition, equation (2), is taken into account, the ion electrochemical potentials of the bulk solution can be substituted by the ion chemical potentials. As a result, $d\Im_V$ can be expressed using the readily available chemical potentials of the external bulk solution, instead of the chemical potentials of the pore solution. If the analysis is restricted to a unidimensional geometry, equation (20) becomes

$$d\Im_V = \sigma\, d\varepsilon + \sum_{k=w,1}^{2} \mu_k \frac{d(e\bar{c}_k)}{1+e_0} \tag{21}$$

The free energy of the solid skeleton, which accounts for the interaction with the fluid phase, $\Im_V^{sk}$, can be derived by subtracting, from $\Im_V$, the free energy of the fluid phase that is given as a function of the specific free energies of the components of the external bulk solution, F_k ($k = w, 1, 2$), to give

$$\Im_V^{sk} = \Im_V - \frac{e}{1+e_0}\sum_{k=w,1}^{2}(\bar{c}_k F_k) \tag{22}$$

The free energy change, due to the interaction between the solid skeleton charge and the ions in the pore solution, is included in $\Im_V^{sk}$ because the specific free energy of the equilibrium bulk solution is subtracted from $\Im_V$, instead of the specific free energy of the pore solution.

Using the thermodynamic relations

$$\mu_k = F_k + \frac{u_k}{c_k} \quad k = w, 1, 2 \tag{23}$$

$$d\mu_k = \frac{du_k}{c_k} \quad k = w, 1, 2 \tag{24}$$

$$dF_k = -u_k d\left(\frac{1}{c_k}\right) \quad k = w, 1, 2 \tag{25}$$

where u_k represents the partial pressure of the kth component of the bulk solution, the change in $\Im_V^{sk}$ can be expressed as

$$d\Im_V^{sk} = \sigma\, d\varepsilon + \sum_{k=w,1}^{2} \frac{u_k}{1+e_0} d\left(\frac{e\bar{c}_k}{c_k}\right) \tag{26}$$

Observing that $\bar{c}_w \cong c_w$ and

$$u_w = u - \Pi \tag{27}$$

where the osmotic pressure represents the sum of the ion partial pressures

$$\Pi = \sum_{i=1}^{2} u_i \tag{28}$$

the increment $d\Im_V^{sk}$ can be expressed as

$$d\Im_V^{sk} = \sigma\, d\varepsilon + (u-\Pi)\frac{de}{1+e_0} + \sum_{i=1}^{2}\frac{u_i}{1+e_0} d\left(\frac{e\bar{c}_i}{c_i}\right) \tag{29}$$

For infinitesimal strains, assuming that the solid component is incompressible

$$d\varepsilon = -\frac{de}{1+e_0} \tag{30}$$

and, as a consequence, equation (29) can be expressed as

$$d\Im_V^{sk} = [\sigma - (u-\Pi)]d\varepsilon + \sum_{i=1}^{2}\frac{u_i}{1+e_0} d\left(\frac{e\bar{c}_i}{c_i}\right) \tag{31}$$

In order to derive the mechanical constitutive equations, it is convenient to work with the Gibbs free energy, G_V^{sk}, which is the following Legendre transform of $\Im_V^{sk}$

$$G_V^{sk} = [\sigma - (u-\Pi)]\varepsilon + \sum_{i=1}^{2}\frac{e}{1+e_0} u_i \frac{\bar{c}_i}{c_i} - \Im_V^{sk} \tag{32}$$

Taking into account equations (31) and (24), the infinitesimal increment in G_V^{sk} is given by

$$\begin{aligned} dG_V^{sk} &= \varepsilon[d\sigma - (du - d\Pi)] + \sum_{i=1}^{2}\frac{e\bar{c}_i}{1+e_0} d\mu_i \\ &= \varepsilon[d\sigma - (du - d\Pi)] + \left[\frac{e(\bar{c}_1 + \bar{c}_2)}{1+e_0}\right]\frac{1}{\nu_1+\nu_2} d\mu_s \end{aligned} \tag{33}$$

where $d\mu_s$ is the salt chemical potential increment, which is defined as

$$\begin{aligned} d\mu_s &= \nu_1 d\mu_1 + \nu_2 d\mu_2 \\ &= \frac{1}{c_s} d\Pi \end{aligned} \tag{34}$$

The function G_V^{sk} can be considered to depend on the variables $[\sigma - (u - \Pi)]$ and μ_s: therefore the simplest constitutive equations that can be inferred are

$$d\varepsilon = \beta_{vv}[d\sigma - (du - d\Pi)] + \beta_{vs} d\mu_s \tag{35}$$

$$\frac{d[e(\bar{c}_1 + \bar{c}_2)]}{(\nu_1 + \nu_2)(1 + e_0)} = \beta_{sv}[d\sigma - (du - d\Pi)] + \beta_{ss} d\mu_s \tag{36}$$

Symmetry of the coefficients (i.e. $\beta_{vs} = \beta_{sv}$) can be demonstrated by considering G_V^{sk} as a continuous function of the variables $[\sigma - (u - \Pi)]$ and μ_s (Dominijanni & Manassero, 2012a).

Equation (35) can also be expressed in the form

$$d\sigma - du - du_{sw} = M d\varepsilon \tag{37}$$

where $M = 1/\beta_{vv}$ is the unidimensional elastic modulus of the porous medium and du_{sw} represents the swelling pressure increment, which is given by

$$du_{sw} = -\varpi d\Pi \tag{38}$$

where $\varpi = 1 + (\beta_{vs}/\beta_{vv}c_s)$ is the swelling coefficient (Dominijanni & Manassero, 2012a).

Since it is known, from experimental observations, that the swelling pressure tends to zero when $c_s \to \infty$, the swelling pressure, u_{sw}, can be obtained as

$$u_{sw} = \int_{\Pi}^{\infty} \varpi d\Pi \tag{39}$$

The effective stress principle can be restored, on the basis of equation (37), if the effective stress increment, $d\sigma'$, is defined as

$$d\sigma' = d\sigma - du - du_{sw} \tag{40}$$

The classical definition of effective stress, $d\sigma' = d\sigma - du$, corresponds to the particular case for which $du_{sw} = 0$, that is, $\varpi = 0$ and $\beta_{vs} = -\beta_{vv}c_s$.

Adopting Donnan's assumptions and using equation (14), the swelling coefficient can be expressed as

$$\varpi = 1 - \frac{d\bar{\Pi}}{d\Pi} \tag{41}$$

Dominijanni & Manassero (2012b) have demonstrated that equation (41) can also be expressed in the form

$$\begin{aligned} \varpi &= 1 - \frac{d\bar{\Pi}}{d\Pi} \\ &= 1 - \frac{\nu_1 + \nu_2}{\nu_1\Gamma_2 + \nu_2\Gamma_1}\Gamma_1\Gamma_2 \end{aligned} \tag{42}$$

Transport equations

If clay is interposed between two reservoirs with different hydraulic pressures or ion concentrations, a pore solution volumetric flux, q, and an ion mass flux, J_i, relative to the solid skeleton, are generated. In order to derive appropriate flux equations, the linear momentum balance equations of the fluid components can be developed on the basis of a number of assumptions. If only unidimensional problems are considered and inertial effects are neglected, these equations can be expressed as (Ehlers, 2002; Dominijanni & Manassero, 2010)

$$-\frac{\partial(n\overline{u}_w)}{\partial x} + f_w = m_w \tag{43}$$

$$-\frac{\partial(n\overline{u}_i)}{\partial x} + f_i = m_i \quad i = 1, 2 \tag{44}$$

where n is the porosity, x is the spatial coordinate, f_w is the external force per unit volume acting on the water, m_w is the momentum supply of water, f_i is the external force per unit volume acting on the ith ion, and m_i is the momentum supply of the ith ion.

The external forces are gravity, which can be considered only to act on the solvent (i.e. water) in the x direction, and the electric force, which is proportional to the electric potential gradient.

$$f_w = n\rho_w \boldsymbol{g} \tag{45}$$

$$f_i = -n\bar{c}_i z_i F \frac{\partial\bar{\phi}}{\partial x} \quad i = 1, 2 \tag{46}$$

where ρ_w is the water density and $\boldsymbol{g}$ is the gravitational acceleration.

The momentum supply of the fluid components can be expressed as

$$m_k = -\bar{u}_k \nabla n + m_k^E \quad k = w, 1, 2 \tag{47}$$

where m_k^E represents the extra-momentum supply of the kth fluid component, which can be associated with the friction between the porous medium components that move with different velocities.

If the extra-momentum supply is associated with the frictional force per unit volume exchanged with the other components of the porous medium, it can be assumed to be equal to the sum of the binary interactions

$$m_w^E = m_{w,sk}^E + \sum_{i=1}^{2} m_{w,i}^E \tag{48}$$

$$m_i^E = m_{i,w}^E + m_{i,j}^E + m_{i,sk}^E \quad i, j = 1, 2;\ i \neq j \tag{49}$$

where w is the water, sk the solid skeleton, and i and j are the ith and jth ions. The friction between the ions and between the ions and the solid skeleton can be considered negligible for a dilute solution compared with the friction between the ions and the solvent

$$\begin{aligned} &m_{i,j}^E;\ m_{i,sk}^E \ll m_{i,w}^E \quad i, j = 1, 2;\ i \neq j \\ &m_i^E \cong m_{i,w}^E \quad i = 1, 2 \end{aligned} \tag{50}$$

Moreover, on the basis of the assumption of binary interaction, it can be assumed that

$$m_{w,i}^E = -m_{i,w}^E \quad i = 1, 2 \tag{51}$$

For the friction forces per unit volume, the following constitutive equations can be adopted.

$$m_{w,sk}^E = \alpha n(v_w - v_{sk}) = \alpha q \tag{52}$$

$$m_{i,w}^E = -m_{w,i}^E = \beta_i n\bar{c}_i(v_i - v_w) \quad i = 1, 2 \tag{53}$$

where α and β_i are friction coefficients, and v_w, v_{sk} and v_i are the water, solid skeleton and ith ion velocities respectively.

The factors n and $(v_w - v_{sk})$ in equation (52), as well as $n\bar{c}_i$ and $(v_i - v_w)$ in equation (53), have been picked out as an indication of the fact that $m_{w,sk}^E = 0$ if $n = 0$ or

$(v_w - v_{sk}) = 0$, and $m^E_{i,w} = 0$ if $n\bar{c}_i = 0$ or $(v_i - v_w) = 0$. However, this does not mean that the friction coefficients α and β_i are independent of n, $\bar{c}_i$ and the relative velocities.

Taking into account these constitutive assumptions, and using the thermodynamic relation that relates the chemical potentials to the partial pressure

$$d\bar{\mu}_k = \frac{d\bar{u}_k}{\bar{c}_k} \quad k = w, 1, 2 \tag{54}$$

the following flux equations can be derived from equations (43) and (44).

$$\begin{aligned} q &= n(v_w - v_{sk}) \\ &= -\frac{n}{\alpha}\left(\bar{c}_w \frac{\partial \bar{\mu}_w}{\partial x} - \rho_w g + \sum_{i=1}^{2} \bar{c}_i \frac{\partial \bar{\mu}_i^{ec}}{\partial x}\right) \end{aligned} \tag{55}$$

$$\begin{aligned} J_i &= n\bar{c}_i(v_i - v_{sk}) \\ &= q\bar{c}_i - n\frac{D_i}{RT}\bar{c}_i \frac{\partial \bar{\mu}_i^{ec}}{\partial x} \quad i = 1, 2 \end{aligned} \tag{56}$$

where $D_i = RT/\beta_i$ represents the macroscopic diffusion coefficient of the ith ion.

At this point, it is convenient to introduce the concept of a virtual external bulk solution that is in thermodynamic equilibrium with the pore solution at the generic position x within the porous medium (Dormieux *et al.*, 1995; Yaroshchuk, 1995). The virtual solution coincides with the real bulk solutions in contact with the porous medium at the boundaries. The thermodynamic potentials in equations (55) and (56) can be substituted with the corresponding potentials of this virtual solution, using equations (6) and (7). This leads to a formulation that does not depend on the determination of the pore solution variables. Therefore, equations (55) and (56) can be expressed as

$$q = -\frac{n}{\alpha}\left(\frac{\partial u}{\partial x} - \frac{\partial \Pi}{\partial x} - \rho_w g + RT\sum_{i=1}^{2}\Gamma_i \frac{\partial c_i}{\partial x} + F\frac{\bar{c}_{sk,0}}{e}\frac{\partial \phi}{\partial x}\right) \tag{57}$$

$$J_i = q\Gamma_i c_i - nD_i\Gamma_i \frac{\partial c_i}{\partial x} - z_i\Gamma_i c_i \frac{nD_i}{RT}F\frac{\partial \phi}{\partial x} \quad i = 1, 2 \tag{58}$$

If an external electric current is not applied to the porous medium, the electric potential derivative in equations (57) and (58) can be eliminated by means of the condition of electric current, I_e, equal to zero.

$$I_e = F\sum_{i=1}^{2} z_i J_i = 0 \tag{59}$$

The resulting flux equations can be expressed as follows

$$q = -\frac{k}{\gamma_w}\left(\frac{\partial u}{\partial x} - \omega\frac{\partial \Pi}{\partial x}\right) \tag{60}$$

$$J_s = (1-\omega)qc_s - nD^*_\omega \frac{\partial c_s}{\partial x} \tag{61}$$

where

$$k = \frac{n\gamma_w}{\alpha\left[1 + \frac{RT}{\alpha}\frac{(\Gamma_1 - \Gamma_2)^2 \nu_1\nu_2 c_s}{\nu_1\Gamma_2 D_2 + \nu_2\Gamma_1 D_1}\right]} \tag{62}$$

$$\omega = 1 - \frac{\nu_1 D_2 + \nu_2 D_1}{\nu_1\Gamma_2 D_2 + \nu_2\Gamma_1 D_1}\Gamma_1\Gamma_2 \tag{63}$$

$$J_s = \frac{J_1}{\nu_1} = \frac{J_2}{\nu_2} \tag{64}$$

$$D^*_\omega = (1-\omega)D_s \tag{65}$$

$$D_s = \frac{(\nu_1 + \nu_2)D_1 D_2}{\nu_1 D_2 + \nu_2 D_1} \tag{66}$$

where k is the hydraulic conductivity, ω is the reflection coefficient, J_s is the salt molar flux, D^*_ω is the osmotic effective diffusion coefficient, and D_s is the macroscopic salt diffusion coefficient.

Dominijanni & Manassero (2012b) have demonstrated that, if the microscopic deviations of the variables from their average values are assumed to be negligible, the macroscopic ion diffusion coefficients, D_i, are equal to the ion effective diffusion coefficients, D^*_i

$$D_i = D^*_i = \tau_m D_{i,0} \quad i = 1, 2 \tag{67}$$

$$\begin{aligned} D_s = D^*_s &= \frac{(\nu_1 + \nu_2)D^*_1 D^*_2}{\nu_1 D^*_2 + \nu_2 D^*_1} \\ &= \tau_m \frac{(\nu_1 + \nu_2)D_{1,0}D_{2,0}}{\nu_1 D_{2,0} + \nu_2 D_{1,0}} \\ &= \tau_m D_{s,0} \end{aligned} \tag{68}$$

where τ_m is the dimensionless matrix tortuosity factor, which accounts for the tortuous nature of the actual diffusive pathway through the porous medium (Malusis & Shackelford, 2002b); $D_{i,0}$ is the free (aqueous) solution diffusion coefficient of the ith ion; D^*_s is the salt effective diffusion coefficient; and $D_{s,0}$ is the free-solution diffusion coefficient of the salt.

An interesting observation is that the reflection coefficient, ω, results as equal to the swelling pressure coefficient, ϖ, when the ion free-solution diffusion coefficients are equal.

When the solid skeleton electric charge is equal to zero, the ion partition coefficients, Γ_i, are equal to 1, and equations (60) and (61) reduce to the Darcy equation and the classical advective diffusion equation respectively.

The osmotic effective diffusion coefficient, D^*_ω, results as related to the reflection coefficient, ω, through equation (65), so that $D^*_\omega = 0$ when $\omega = 1$. As a result, the condition $\omega = 1$ implies a null salt flux through the porous medium, which in this case can be said to act as a 'perfect' or 'ideal' barrier.

If equation (65) is compared with the expression for D^*_ω proposed by Malusis & Shackelford (2002b) and Malusis *et al.* (2012)

$$D^*_\omega = \tau_r D^*_s \tag{69}$$

where τ_r is the restrictive tortuosity factor, the result is that τ_r is given by

$$\tau_r = (1-\omega)\frac{D_s}{D^*_s} \tag{70}$$

Moreover, if the hypotheses implied by equation (68) are adopted, the expression for τ_r reduces to

$$\tau_r = 1 - \omega \tag{71}$$

The coefficient k can be measured, under steady-state conditions, using traditional permeameters. Malusis *et al.* (2001) developed a testing apparatus to determine ω and D^*_ω. This apparatus is able to impose the condition of no volumetric flux ($q = 0$) through a soil sample in contact with two external solutions, maintained at constant salt concentrations, so that the global or averaged values of the coefficients can be measured. The global values of ω and D^*_ω are defined as (Auclair *et al.*, 2002)

$$\omega_g = \frac{1}{\Delta c_s}\int_{c_b}^{c_t} \omega \mathrm{d}c_s \tag{72}$$

$$D^*_{\omega g} = \frac{1}{\Delta c_s}\int_{c_b}^{c_t} D^*_{\omega} \mathrm{d}c_s \tag{73}$$

where c_t and c_b represent the salt concentration at the top and the bottom boundaries of the clay sample respectively, and $\Delta c_s = c_t - c_b$ is their difference. These coefficients can be determined by means of the following relations under steady-state conditions.

$$\omega_g = \left(\frac{\Delta u}{\Delta \Pi}\right)_{q=0} \tag{74}$$

$$D^*_{\omega g} = \frac{L}{n}\left(\frac{J_s}{\Delta c_s}\right)_{q=0} \tag{75}$$

where $\Delta u = u_t - u_b$ and $\Delta \Pi = \Pi_t - \Pi_b$ represent the differences between the hydraulic pressure and the osmotic pressure at the boundaries of the clay sample, and L is the length of the sample.

It is interesting to observe that the relationship between D^*_{ω} and ω is also maintained between their corresponding global values; in fact, inserting equation (65) into equation (73) with $D_s = D^*_s$ leads to

$$\begin{aligned} D^*_{\omega g} &= (1 - \omega_g) D^*_s \\ &= (1 - \omega_g)\tau_m D_{s,0} \end{aligned} \tag{76}$$

For a salt constituted by monovalent ions, inserting equation (63) into equation (72) and using equations (17) and (18), the following expression for ω_g is obtained

$$\omega_g = 1 + \frac{\bar{c}_{sk,0}}{2\Delta c_s e}\left[Z_2 - Z_1 - (2t_1 - 1)\ln\left(\frac{Z_2 + 2t_1 - 1}{Z_1 + 2t_1 - 1}\right)\right] \tag{77}$$

where

$$t_1 = \frac{D_{1,0}}{D_{1,0} + D_{2,0}} \tag{78}$$

$$Z_1 = \sqrt{1 + \left(\frac{2c_t e}{\bar{c}_{sk,0}}\right)^2} \tag{79}$$

$$Z_2 = \sqrt{1 + \left(\frac{2c_b e}{\bar{c}_{sk,0}}\right)^2} \tag{80}$$

and t_1 is the cation transport number.

MATERIALS AND METHODS

Materials

The powdered bentonite tested in this study is an Indian sodium bentonite that is used for the production of a needle-punched GCL. The bentonite is characterised by a cation exchange capacity (CEC, measured using the methylene blue adsorption method) of 105 meq/100 g. The mineralogical composition, evaluated through X-ray diffraction analysis, indicates a bentonite that is composed primarily of smectite (> 98%), with traces of calcite, quartz, mica and gypsum.

The bentonite is characterised by a liquid limit (LL) of 525% and a hydraulic conductivity of 8×10^{-12} m/s, measured at a 27·5 kPa confining effective stress using de-ionised water (DW) as the permeant liquid.

Sodium solutions were prepared with sodium chloride (ACS reagent, purity ⩾ 99%) and DW. The sodium solutions were prepared at different molarity values in the range 5–100 mM, with the aim of investigating the effect of the monovalent cations on the osmotic behaviour of the bentonite. The DW (pH = 6·95; electrical conductivity (EC) at 20°C = 0·6 mS/m) consisted of tapwater processed through a series of activated carbon filters, a reverse osmosis process and, finally, an ultraviolet (UV) lamp (Elix Water Purification system). Moreover, the DW was de-aerated prior to use. The EC measured at 20°C for the sodium chloride solutions ranged from 60·5 mS/m to 1·1 mS/m.

Bentonite preparation. Prior to the osmotic property determination, the bentonite was submitted to a process with the aim of removing the soluble salts (mainly sodium) that are naturally present inside the material, owing to its marine origin. The treatment prevents soluble salts from interfering with the determination of the osmotic properties.

Previous studies (Malusis *et al.*, 2001; Malusis & Shackelford, 2002a, 2002b; Shackelford & Lee, 2003; Yeo *et al.*, 2005; Kang & Shackelford, 2009; Di Emidio, 2010) have used the 'flushing' method to remove soluble salts. This method consists of an initial permeation phase, performed under back-pressure, which requires a long period of time (i.e. from months to a year), because of the low bentonite hydraulic conductivity.

In this study the 'squeezing' method has been used, with the aim of reducing the salt removal time. The squeezing method consists of a series of consecutive phases of powder bentonite hydration with DW, at a higher water content than the LL, and drained consolidation, performed in a consolidometer under a maximum load of 500 kPa. Moreover, the drained solution is sampled daily, and the EC is monitored to evaluate the soluble salt concentration in the bentonite pore water. After the squeezing process, the material is oven-dried at 105°C and pulverised once again. When a 5 l consolidometer is used, the above procedure can produce about 500 g of squeezed dry powder bentonite, characterised by an EC value lower than 50 mS/m, in 40–50 days. The results of the EC monitoring during the squeezing process are reported in Fig. 1.

The specimen for the chemico-osmotic test is prepared by rehydrating the squeezed bentonite with DW at a lower water content than the LL value, and then by statically compacting the material in a compaction mould, while allowing the excess water to be released.

Dry powder bentonite is required for the swelling pressure test.

Testing apparatus and procedures

Chemico-osmotic test. The testing apparatus used to measure the global reflection coefficient and the global osmotic effective diffusion coefficient is described in detail in Malusis *et al.* (2001). The main components of the apparatus, shown in Fig. 2, are the osmotic cell, the flow pump system, the pressure transducer, which is used to measure the differential pressure that develops across the specimen during the test, and the data acquisition system.

The cell consists of a modified rigid-wall permeameter, in which the top piston and the bottom pedestal are equipped with three ports each: two enable the different solutions to circulate through the top (sodium chloride solution) and the bottom (DW) porous stones, with the aim of establishing a constant concentration gradient across the specimen. The third port is installed in both the top piston and the bottom pedestal to allow the differential pressure across the specimen to be measured.

The flow pump system, which consists of a dual-carriage

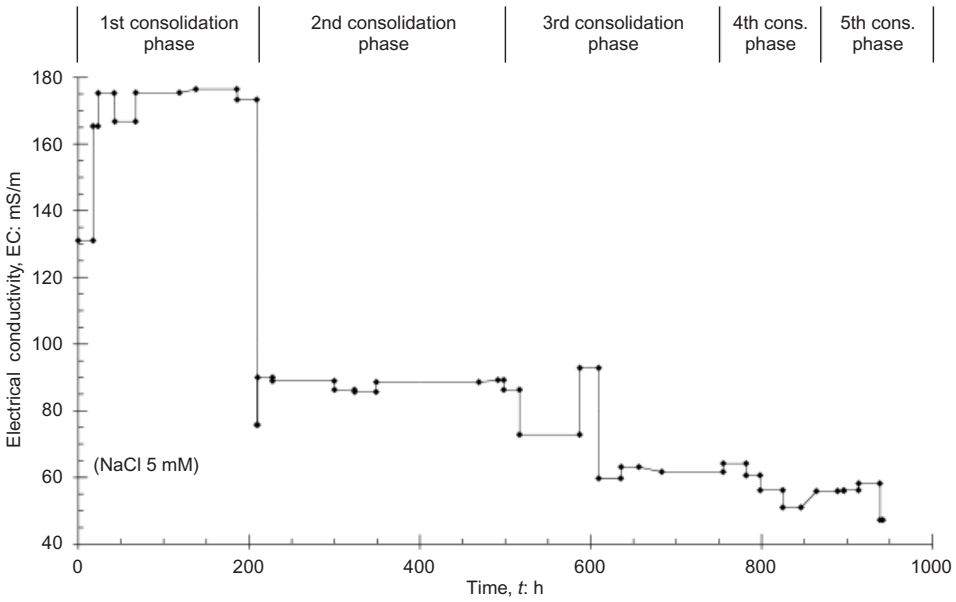

Fig. 1. Electrical conductivity as a function of time during squeezing process

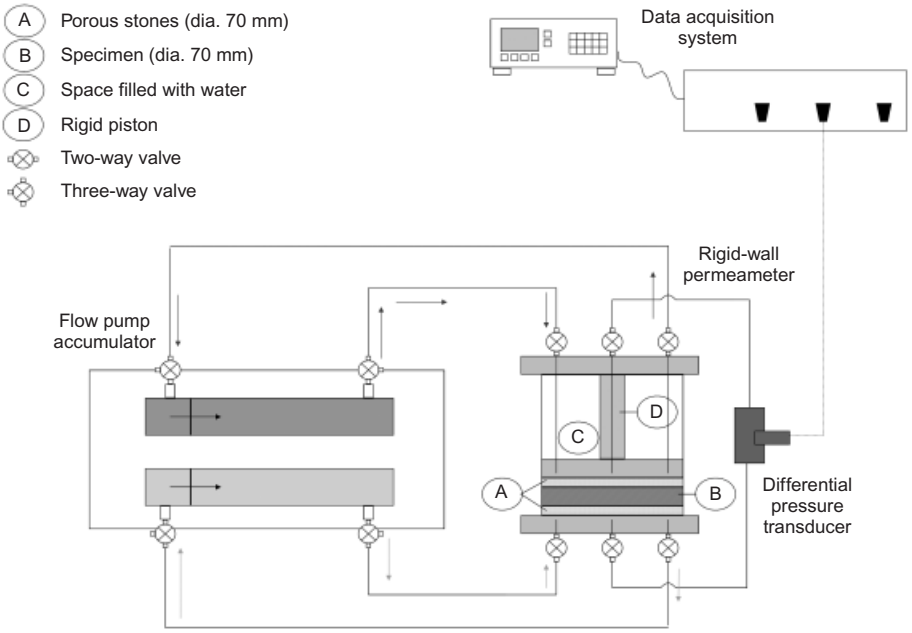

Fig. 2. Schematic view of chemico-osmotic test apparatus. More details on this apparatus can be found in Malusis *et al.* (2001)

syringe pump and two stainless steel accumulators (Model 33 twin syringe pump, produced by Harvard, Holliston, MA), prevents volumetric flux through the specimen by simultaneously injecting into and withdrawing from the porous stones the same volume of solution. In order to obtain this result, the syringes have to move at the same rate.

The test was performed according to the procedure proposed by Malusis *et al.* (2001): a solution containing a known electrolyte concentration (sodium chloride) was circulated in the top porous stone, while DW was circulated in the bottom porous stone. The concentration difference across the specimen was maintained constant by continuously infusing the two liquids at the boundaries of the specimen.

As the specimen was first squeezed with DW to remove the soluble salts, the EC of the electrolyte solutions in the flux exiting from the porous stones at the steady state was induced solely by the contributions of Cl^- and Na^+ ions. Moreover, the calibration reported in Fig. 3 shows that the relation between the EC and solution molarity was linear over the concentration range examined in the study. As a consequence, the EC of the withdrawn fluxes (i.e. from the top and bottom porous stones) was monitored by sampling the solution contained in the pistons, and the sodium chloride molar concentration was derived using a linear relation. Since the volumetric flux through the specimen was hindered, the global reflection coefficient could be calculated using equation (74).

The diffusive solute flux through the specimen was calculated for the nth sampling interval according to

$$J_s^n = \frac{\sum_{m=1}^{n} (c_s^m \Delta V^m)}{A_S \Delta t^n} = \frac{\Delta Q^n}{\Delta t^n} \tag{81}$$

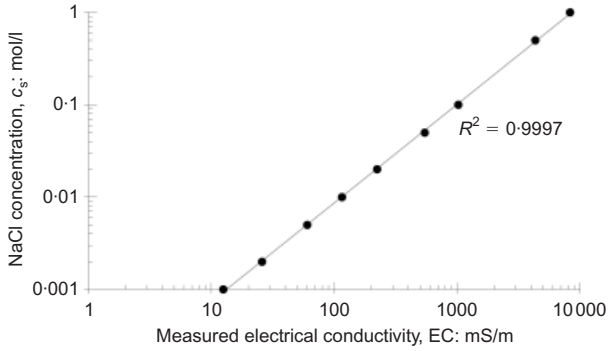

Fig. 3. Calibration of sodium chloride (NaCl) concentration with electrical conductivity. R^2 is coefficient of determination of regression line

where c_s^n is the solute molar concentration measured by sampling the solution coming out from the bottom porous stone, ΔV^m is the volume of the solution circulating in the porous stones in the interval Δt^m, A_S is the cross-section of the specimen, and ΔQ^n is the cumulative salt molar mass per unit area that passed through the specimen. The global osmotic effective diffusion coefficient, $D^*_{\omega g}$, is calculated at the steady state as

$$D^*_{\omega g} = \frac{\Delta Q}{\Delta t} \frac{L}{n\left(c_{t,avg} - c_{b,avg}\right)} \tag{82}$$

where $c_{t,avg}$ and $c_{b,avg}$ are the average top and bottom salt concentrations respectively.

Swelling pressure test. The swelling pressure apparatus, shown in Fig. 4, consists primarily of a stainless steel oedometer cell, a sodium chloride solution supply tank placed above the pressure panel, a displacement transducer connected to the cell top piston, which is used to measure the axial strains of the specimen, a load cell, and a data acquisition system.

The swelling pressure apparatus consists of a rigid cell that confines the sample (i.e. the oedometer), which allows access to the water through both porous stones. The cell is connected to a pressure panel that allows the specimen to be back-pressurised. The rigid piston above the upper porous stone is connected to the load cell, which measures the pressure that has to be applied in order to hinder the axial strain of the specimen.

The test procedure requires a known amount of dry material to be dusted inside the oedometer ring, the cell to be assembled, and a sodium chloride solution to be supplied. The specimen, which is characterised by an initial dry height of 5 mm, is allowed to swell to 10 mm. The piston is then blocked, the sample is back-pressurised, and the steady-state swelling pressure is recorded after a short transitional phase.

Since the bentonite that is initially dusted inside the oedometer is dry, the pressure increases for a number of days during the hydration phase, and the steady-state swelling pressure is reached when hydration has been completed.

RESULTS

Chemico-osmotic test results

The chemico-osmotic test was performed using the oven-dried squeezed material, rehydrated with DW and then

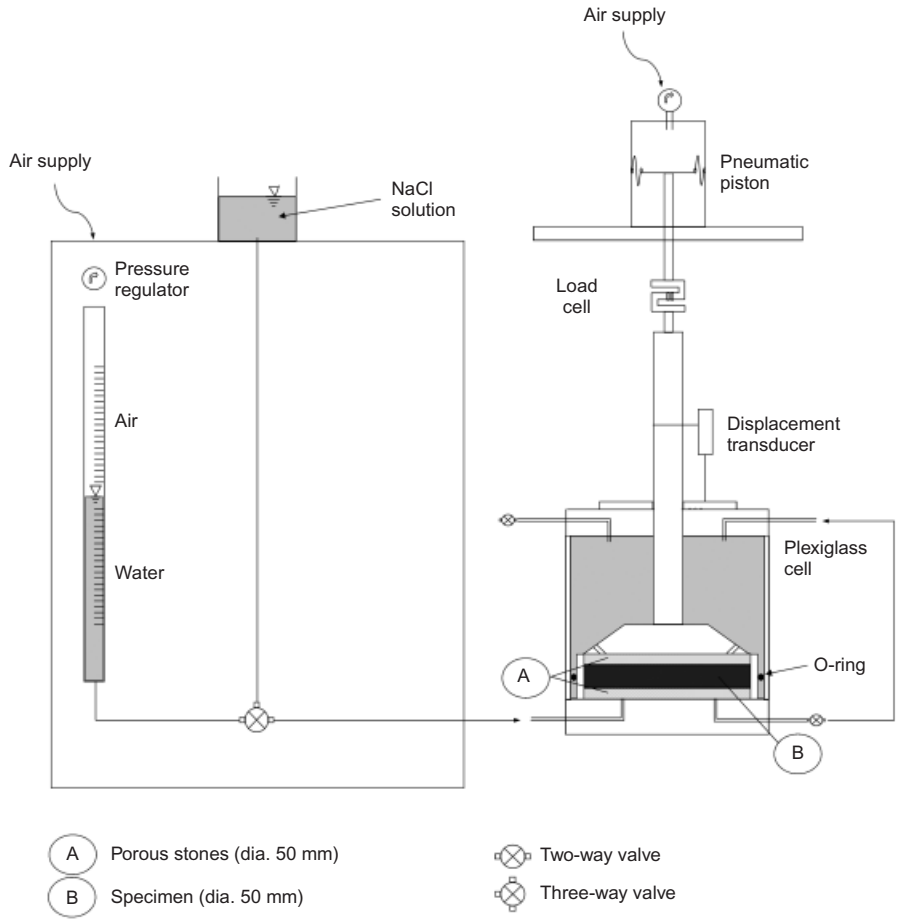

Fig. 4. Schematic view of the swelling pressure apparatus

statically compacted, in a drained compaction mould, at a porosity n equal to 0·81 ($e = 4{\cdot}26$). After the preparation phase, the 17 mm thick specimen was transferred to the cell for the osmotic test.

After assembling the cell, DW was circulated through the top piston and the bottom pedestal for 2 weeks in order to establish a steady baseline differential pressure, before a concentration gradient was applied to the specimen. A source concentration of sodium chloride was then injected into the top porous stone, while DW was continuously circulated in the bottom porous stone.

A multiple-stage chemico-osmotic test was performed by sequential circulation of chemical solutions containing 5·16, 10·27, 20·24, 51·94 and 109·31 mM sodium chloride concentrations at a constant flow rate of 0·05 ml/min.

The EC values of the salt mass fluxes withdrawn from the top and the bottom porous stones, measured during the testing stages, are shown in Fig. 5. The measured values depend on the sodium chloride concentrations imposed at the boundaries of the specimen: the EC values progressively increase during the test as the sodium chloride concentration of the injected solution in the top porous stone rises. The trends of the electrical conductivity of the flux withdrawn from the top porous stone, $EC_{t,exit}$, and of that withdrawn from the bottom porous stone, $EC_{b,exit}$, both show that a steady state has been reached for each stage.

Moreover, the difference between the EC values measured in the flux withdrawn from the top porous stone ($EC_{t,exit}$) and those of the solutions injected into the same stone ($EC_{t,ref}$) is due to the loss in sodium chloride mass induced by the diffusion through the bentonite from the top to the bottom boundary.

The global reflection coefficient values, ω_g, obtained during the multiple-stage chemico-osmotic test, are shown in Fig. 6 as a function of time. The ω_g values are determined using equation (74), on the basis of the differential pressure, Δu, measured during the test with a time step of 10 min, and the osmotic pressure, $\Delta\Pi$, calculated from the average of the top and bottom sodium chloride concentrations. The steady-state values of the variables are reported in Table 1 for each concentration stage. The sodium chloride concentrations were derived from the measured EC using the linear calibration reported in Fig. 3.

As far as the EC measurements are concerned, the trend of the global reflection coefficient shows that a steady state has been reached for each stage. The steady-state ω_g values tend to decrease as the salt concentration in the top porous stone increases. The recorded values range from 68%, for a

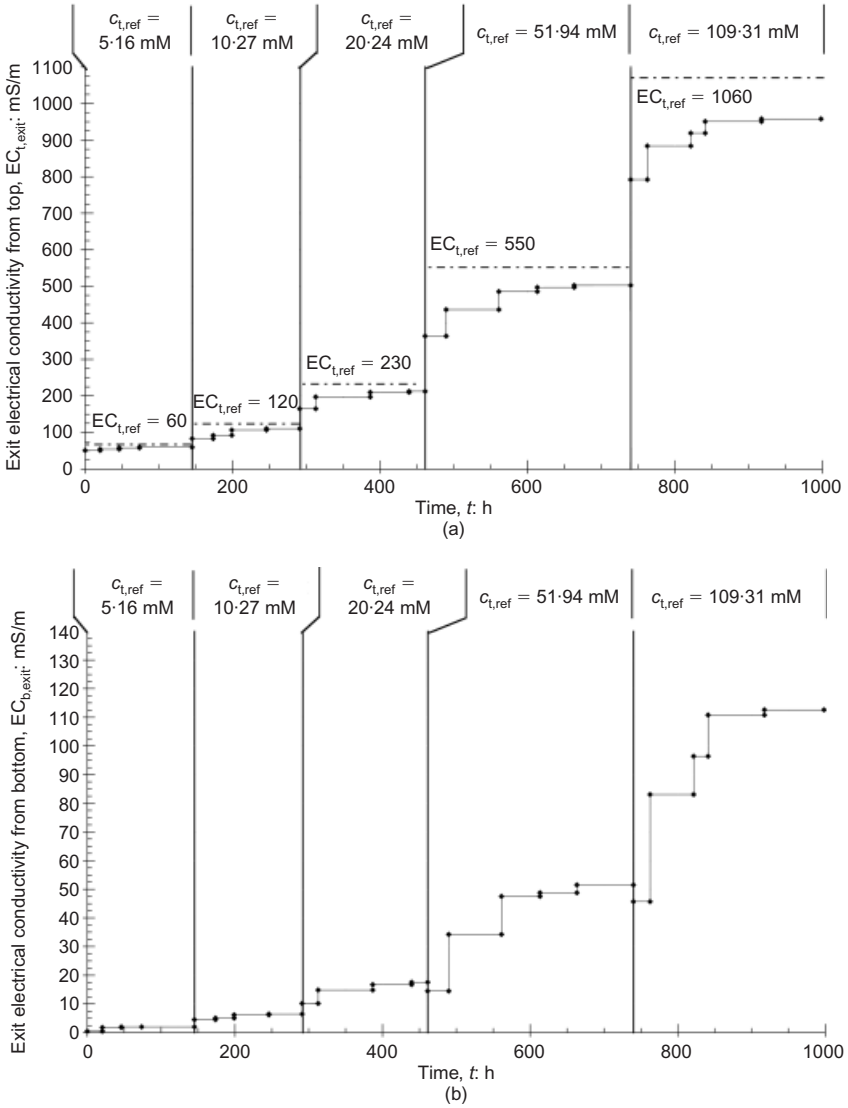

Fig. 5. Electrical conductivity of salt flux withdrawn from (a) top porous stone and (b) bottom porous stone as a function of time during multiple-stage chemico-osmotic test

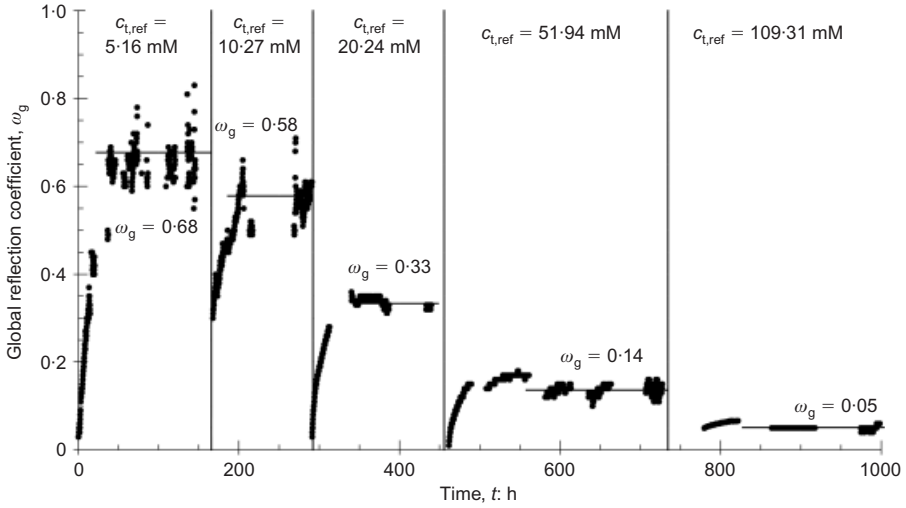

Fig. 6. Global reflection coefficient as a function of time during multiple-stage chemico-osmotic test

Table 1. Steady-state values of variables involved in multiple-stage chemico-osmotic test

$c_{t,ref}$: mM	$c_{t,exit}$: mM	$c_{b,exit}$: mM	$c_{t,avg}$: mM	$c_{b,avg}$: mM	Δu: kPa	$\Delta\Pi$: kPa	ω_g	$D^*_{\omega g}$: m^2/s
5·16	5·12	0·83	5·14	0·42	15·65	23·02	0·68	–
10·27	9·61	0·85	9·94	0·43	26·87	46·33	0·58	$2·54 \times 10^{-10}$
20·24	18·93	1·45	19·58	0·72	30·32	91·89	0·33	$3·52 \times 10^{-10}$
51·94	47·39	4·39	49·67	2·19	32·38	231·30	0·14	$4·19 \times 10^{-10}$
109·31	97·18	9·78	103·24	4·89	23·96	479·21	0·05	$4·60 \times 10^{-10}$

5·16 mM sodium chloride source concentration, to 5%, for a 109·31 mM sodium chloride source concentration. The global reflection coefficient can be assumed approximately null for higher molarities.

The cumulative molar mass per unit area, Q, of the sodium chloride that migrated through the specimen during the multiple-stage test is reported in Fig. 7. The values of the global osmotic effective diffusion coefficient, $D^*_{\omega g}$, which

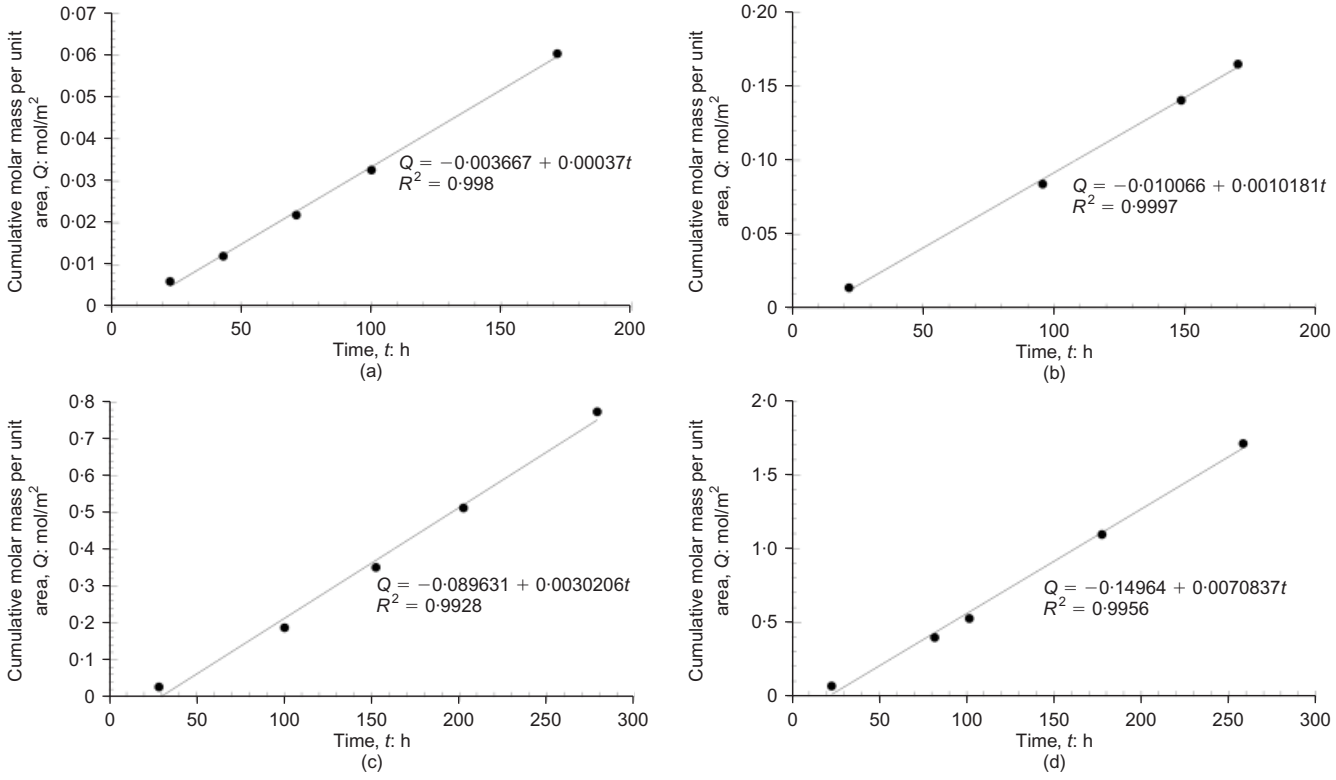

Fig. 7. Cumulative molar mass of sodium chloride per unit area as a function of time during multiple-stage chemico-osmotic test: (a) $c_{t,ref}$ = 10·27 mM; (b) $c_{t,ref}$ = 20·24 mM; (c) $c_{t,ref}$ = 51·94 mM; (d) $c_{t,ref}$ = 109·31 mM

have been obtained from the Q measurements shown in Fig. 7, are reported in Table 1.

Swelling pressure test results

The swelling pressure test was performed using dry specimens, prepared with the squeezed, oven-dried bentonite and characterised by an initial dry height of 5 mm, which were allowed to swell to 10 mm during hydration. The final hydrated volume of the specimens corresponded to $n = 0{\cdot}81$.

The test was performed by hydrating five specimens with five different sodium chloride solutions, characterised by increasing concentrations: 5, 10, 20, 50 and 100 mM. After hydration, the specimen volume change was inhibited, and the value of the swelling pressure was recorded after a short transitional phase.

The swelling pressure trend is reported in Fig. 8 for each test as a function of time. Since, during the tests, the load cell was unloaded until the specimen swelled to 10 mm, the initial swelling/hydration phase of the dry material (from 5 to 10 mm) was characterised by null swelling pressure values.

All the tests show that the swelling pressure increases for approximately 15–20 h, during the controlled hydration phase (i.e. when the volumetric strain is inhibited), and that the equilibrium swelling pressure is reached when the hydration phase is completed. Moreover, in the tests with lower sodium chloride concentrations (i.e. for 5 and 10 mM sodium chloride equilibrium solutions), the specimens were successively back-pressurised to 300 kPa. The obtained results show that the swelling pressure value does not change after back-pressurisation.

In the test performed using the 100 mM sodium chloride solution, the bentonite specimen did not rise to 10 mm, as it stopped at a height of 9·5 mm, and the load cell was never loaded during the test. For this reason, the swelling pressure for this test was taken equal to zero.

INTERPRETATION OF TEST RESULTS

The experimental results can be related to the physical and chemical properties of the tested bentonite under the assumption that the microscopic deviations of the state variables from their average values are negligible. In such a case, both the global reflection coefficient and the swelling pressure depend on the solid skeleton electric charge through equations (19) and (77). Therefore, from the best-fitting of the theoretical curves with the experimental data of both tests, a value of $\bar{c}_{sk,0}$ equal to 90 mM was found. The obtained theoretical curves are reported in Figs 9 and 10, together with the experimental data.

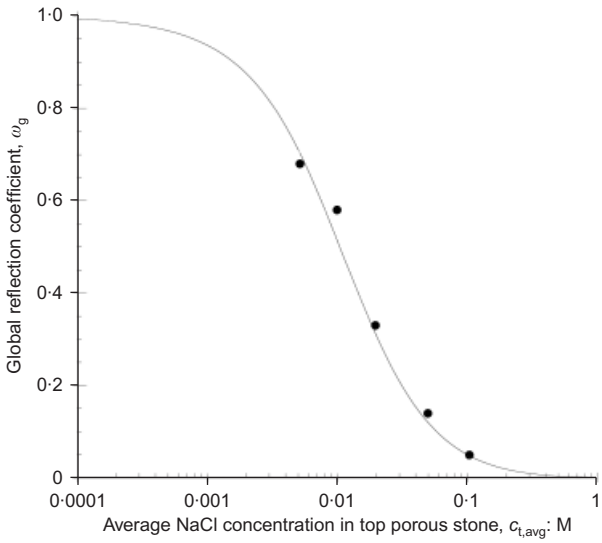

Fig. 9. Global reflection coefficient, ω_g, as a function of average sodium chloride (NaCl) concentration at top boundary of bentonite specimen, with best-fitting theoretical curve, obtained for $\bar{c}_{sk,0} = 90$ mM in equation (77) (continuous line)

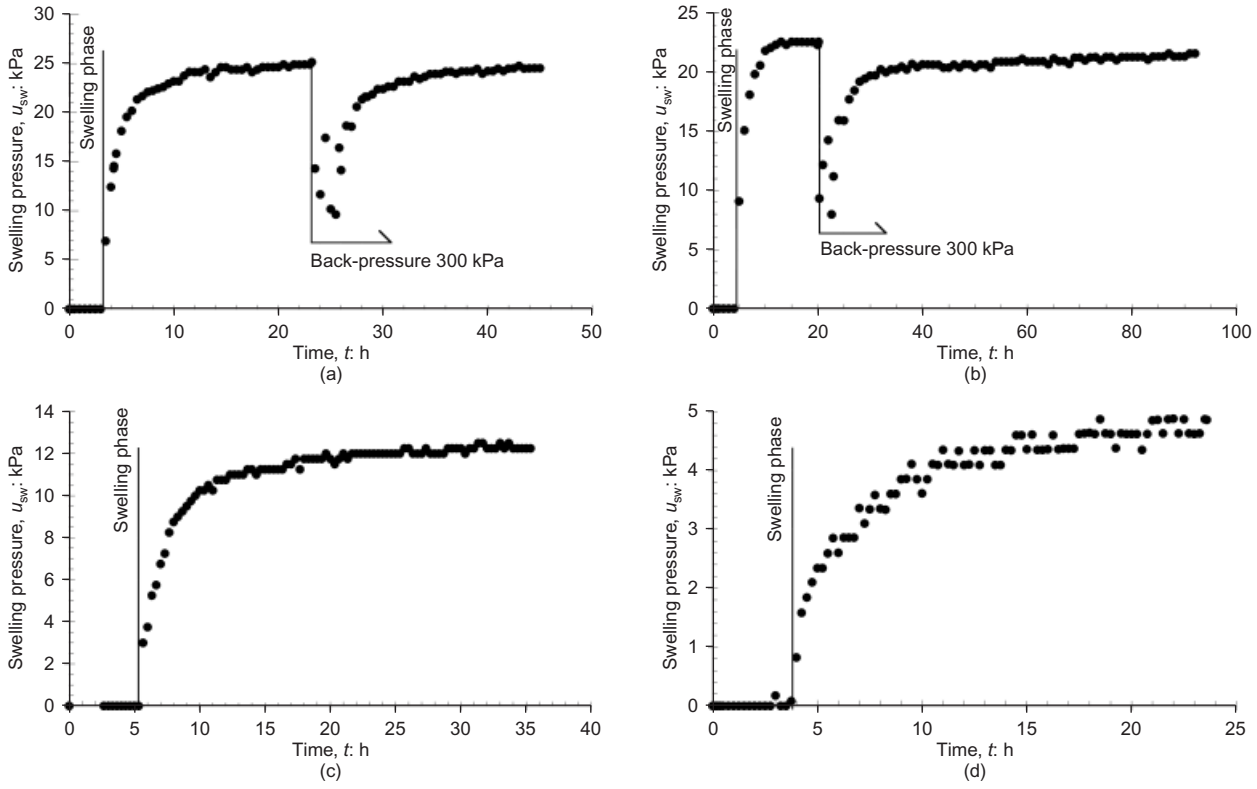

Fig. 8. Swelling pressure as a function of time. (a) $c_s = 5$ mM; (b) $c_s = 10$ mM; (c) $c_s = 20$ mM; (d) $c_s = 50$ mM

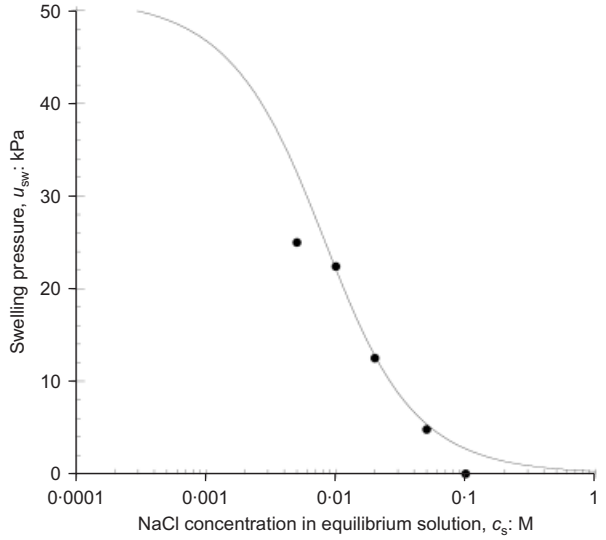

Fig. 10. Swelling pressure, u_{sw}, as a function of sodium chloride (NaCl) equilibrium concentration, with best-fitting theoretical curve, obtained for $\bar{c}_{sk,0} = 90$ mM in equation (19) (continuous line)

The salt concentration at the top boundary was taken equal to $c_{t,avg}$ to determine ω_g, and the salt concentration at the bottom boundary was considered equal to zero: that is, $c_b \cong c_{b,avg} \cong 0$. The sodium transport number was calculated from the sodium and chloride free-solution diffusion coefficient values (Shackelford & Daniel, 1991): $D_{Na,0} = 13{\cdot}3 \times 10^{-10}$ m^2/s, $D_{Cl,0} = 20{\cdot}3 \times 10^{-10}$ m^2/s.

In Fig. 11, the experimental reflection coefficient data were also fitted with the empirical semi-log linear curve proposed by Shackelford *et al.* (2003) and Malusis *et al.* (2003),

$$\omega_g = A + B \log (c_{t,avg}) \tag{83}$$

where A and B are the regression parameters. The value of the coefficient of determination R^2 close to 1 confirms the ability of this empirical curve to fit the ω_g experimental data, as was found by Malusis *et al.* (2003) for the Kemper & Rollins (1966) and Malusis & Shackelford (2002a) data. However, the regression parameters A and B should be intended as functions of the soil porosity (Malusis *et al.*, 2003) and of the bottom boundary condition (i.e. $c_{b,avg}$). The advantage of interpreting the experimental data with the proposed theoretical model is that, when the single unknown parameter, $\bar{c}_{sk,0}$, has been calibrated on a restricted experimental dataset, the global reflection coefficient values can be estimated for different soil porosities and boundary conditions through equation (77).

The tortuosity factor was determined by plotting the measured values of $D^*_{\omega g}$ as a function of the corresponding values of the complement to 1 of ω_g – that is, $(1 - \omega_g)$ – and finding the intercept of the linear regression with the ordinate axis at $(1 - \omega_g) = 1$ – that is, $\omega_g = 0$ (Fig. 12). The tortuosity factor in equation (76) is in fact given by

$$\tau_m = \left(\frac{D^*_{\omega g}}{D_{s,0}} \right)_{\omega_g = 0} \tag{84}$$

where $D_{s,0}$ is the sodium chloride free-solution diffusion coefficient, which is equal to 16×10^{-10} m^2/s (Shackelford & Daniel, 1991).

A value of τ_m equal to 0·31 was obtained from the data plotted in Fig. 12. The resulting theoretical curve of $D^*_{\omega g}$ is reported in Fig. 13 as a function of the top boundary salt concentration.

The obtained values of $\bar{c}_{sk,0}$ and τ_m are compared in Table 2 with those derived by Dominijanni & Manassero (2012b) from the interpretation of the experimental results of Malusis & Shackelford (2002a, 2002b), relative to a geosynthetic clay liner, with a bentonite porosity, n, of 0·79 for different concentrations of potassium chloride (KCl). The differences in the parameters obtained from the two studies can be attributed both to the different mineralogical compositions of the tested bentonites and to the different salts contained in the pore solutions.

The theoretical linear relationship between $D^*_{\omega g}$ and $(1 - \omega_g)$ in Fig. 12 is a consequence of assuming that the pore-scale variations in the hydraulic pressure, ion concentrations and water velocity within the soil are negligible; as a result, the agreement of the experimental data with the linear relationship is an indication of the acceptability of this assumption.

The goodness of the linear fitting shown in Fig. 12 ($R^2 = 0{\cdot}9810$) and the possibility of fitting both the global reflection coefficient and the swelling pressure data with a single value of $\bar{c}_{sk,0}$ are indications of the ability of the

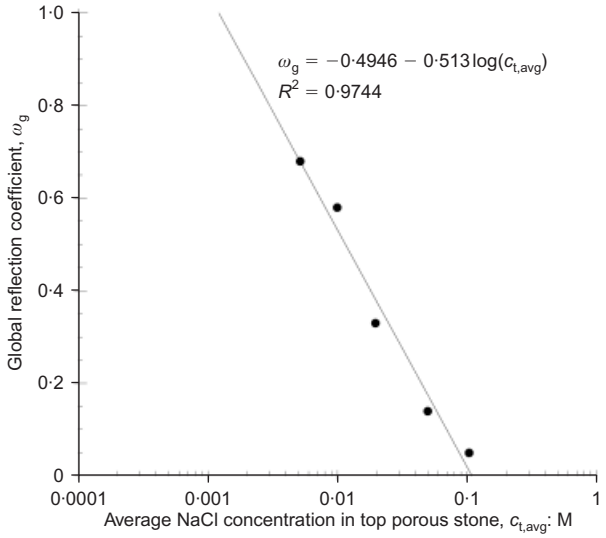

Fig. 11. Semi-log linear regression of measured global reflection coefficients against average sodium chloride (NaCl) concentration at top boundary of bentonite specimen

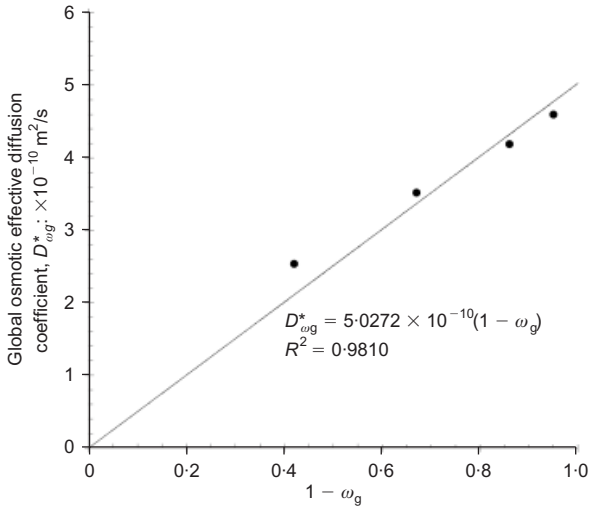

Fig. 12. Global osmotic effective diffusion coefficient, $D^*_{\omega g}$, as a function of the complement to 1 of the global reflection coefficient, ω_g, with theoretical linear relation given by equation (76) (continuous line)

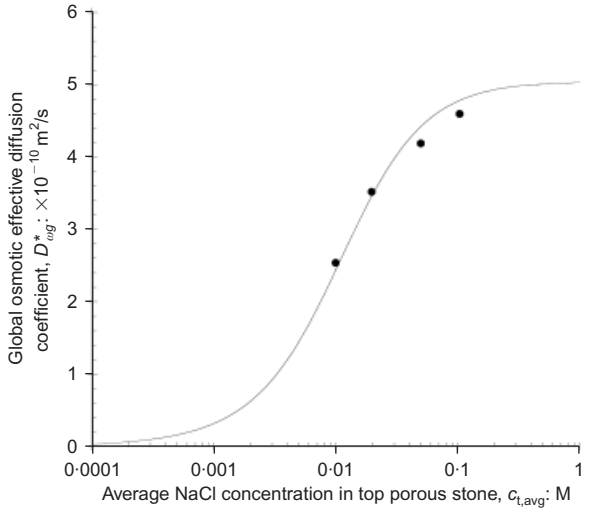

Fig. 13. Global osmotic effective diffusion coefficient, $D^*_{\omega g}$, as a function of average sodium chloride (NaCl) concentration at top boundary of bentonite specimen, with the best-fitting theoretical curve, obtained for $\bar{c}_{sk,0} = 90$ mM and $\tau_m = 0{\cdot}31$ in equations (76) and (77) (continuous line)

proposed theoretical approach to simulate the bentonite behaviour.

CONCLUSIONS

A theoretical approach that takes into account the interaction between the electric charge of the bentonite solid skeleton and the ions contained in the pore solution has been proposed. The phenomenological parameters introduced in this theoretical approach were measured for a bentonite specimen with porosity, n, of 0·81, over a range of sodium chloride concentrations in the pore solution varying from 5 mM to 100 mM. Both the global reflection coefficient, ω_g, and the swelling pressure, u_{sw}, were found to decrease with an increase in the salt concentration. This result is in agreement with the trends given by the proposed theoretical model, assuming that the microscopic deviations of the pore solution state variables from their average values are negligible. If this assumption is accepted, the experimental data can be used to derive the electric charge of the solid skeleton (per unit solid volume), $\bar{c}_{sk,0}$, and the tortuosity factor, τ_m. The mechanical behaviour and the transport properties of bentonite can be estimated from these physical properties to evaluate its performance as a hydraulic and contaminant barrier in field applications. However, in order to verify the applicability of the proposed model under different boundary conditions and for different salts contained in the pore solution, further experimental evaluations must be conducted. Moreover, the results obtained for a single salt contained in the bentonite pore solution need to be extended to the more general problem of a solution containing an unspecified number of salts, in order to evaluate the performance of bentonites that are used as contaminant barriers for real leachates.

NOTATION

A, B	regression parameters
A_S	cross-section of specimen
c_b	salt concentration at bottom boundary of specimen
$c_{b,avg}$	average salt concentration at bottom boundary of specimen
$c_{b,exit}$	salt concentration of flux withdrawn from bottom porous stone
c_i	molar concentration of ith ion in equilibrium bulk solution
$\bar{c}_i$	molar concentration of ith ion in pore solution
c_k	molar concentration of kth fluid component in equilibrium bulk solution
$\bar{c}_k$	molar concentration of kth fluid component in pore solution
c_s	salt molar concentration in equilibrium bulk solution
Δc_s	salt concentration difference
$\bar{c}_{sk,0}$	molar concentration per unit solid volume of solid skeleton electric charge
c_t	salt concentration at top boundary of specimen
$c_{t,avg}$	average salt concentration at top boundary of specimen
$c_{t,exit}$	salt concentration of flux withdrawn from top porous stone
$c_{t,ref}$	source salt concentration
c_w	water molar concentration in equilibrium bulk solution
$\bar{c}_w$	water molar concentration in pore solution
D_i	macroscopic diffusion coefficient of ith ion
$D_{i,0}$	free (aqueous) solution diffusion coefficient of ith ion
D^*_i	effective diffusion coefficient of ith ion
D_s	macroscopic salt diffusion coefficient
$D_{s,0}$	free (aqueous) solution salt diffusion coefficient
D^*_s	effective salt diffusion coefficient
D^*_ω	osmotic effective diffusion coefficient
$D^*_{\omega g}$	global osmotic effective diffusion coefficient
$EC_{b,exit}$	electrical conductivity of flux withdrawn from bottom porous stone
$EC_{t,exit}$	electrical conductivity of flux withdrawn from top porous stone
$EC_{t,ref}$	electrical conductivity of source solution
e	void ratio
e_0	initial void ratio
F	Faraday's constant (96 485 C/mol)
F_k	free energy per unit molar mass of kth component of fluid phase

Table 2. Comparison between physical parameters derived from interpretation of experimental results in this work and those obtained by Dominijanni & Manassero (2012b) from interpretation of tests carried out by Malusis & Shackelford (2002a, 2002b)

Experimental data	Material	Method for removing soluble salts	Tests	Salt in pore solution	Porosity, n	Solid skeleton charge concentration, $\bar{c}_{sk,0}$: mM	Tortuosity factor, τ_m
This study	Natural sodium bentonite	Squeezing	Chemico-osmotic test and swelling pressure test	NaCl	0·81	90	0·31
Malusis & Shackelford (2002a, 2002b)	Geosynthetic clay liner containing natural sodium bentonite	Flushing	Chemico-osmotic test	KCl	0·79–0·80	46	0·14

f_i external force per unit volume acting on ith ion
f_w external force per unit volume acting on water
G_V^{sk} Gibbs free energy of solid skeleton per unit (undeformed) volume of porous medium
$\boldsymbol{g}$ gravitational acceleration
I_e electric current density
$\Im_V$ free energy per unit (undeformed) volume of porous medium
$\Im_V^{sk}$ free energy of solid skeleton per unit (undeformed) volume of porous medium
J_i molar flux of ith ion relative to solid skeleton
J_s salt molar flux
k hydraulic conductivity
L length of specimen
M unidimensional elastic modulus of porous medium
m_i momentum supply of ith ion
m_i^E extra-momentum supply of ith ion
m_k momentum supply of kth fluid component
m_k^E extra-momentum supply of kth fluid component
$m_{l,m}^E$ extra-momentum supply exchanged between lth and mth components of porous medium (sk = solid skeleton, w = water, 1 = cation, 2 = anion)
m_w momentum supply of water
n porosity
Q cumulative salt molar mass per unit area
ΔQ increment in cumulative salt molar mass per unit area
q water volumetric flux relative to solid skeleton
R universal gas constant (= 8·314 J/(mol K))
T absolute temperature in equilibrium bulk solution
$\bar{T}$ absolute temperature in pore solution
t time
Δt time interval
t_1 cation transport number
u hydraulic pressure in equilibrium bulk solution
Δu hydraulic pressure difference
$\bar{u}$ hydraulic pressure in pore solution
u_b hydraulic pressure at bottom boundary of specimen
u_i partial pressure of ith ion component in equilibrium bulk solution
$\bar{u}_i$ partial pressure of ith ion component in pore solution
u_k partial pressure of kth fluid component in equilibrium bulk solution
$\bar{u}_k$ partial pressure of kth fluid component in pore solution
u_{sw} swelling pressure
u_t hydraulic pressure at top boundary of porous medium
u_w partial pressure of water in equilibrium bulk solution
$\bar{u}_w$ partial pressure of water in pore solution
ΔV^m volume of solution circulating in porous stones
v_i velocity of ith ion
v_{sk} velocity of solid skeleton
v_w water velocity
x spatial coordinate
z_i electrochemical valence of ith ion
z_{sk} electrochemical valence of solid skeleton electric charge
α, β_i friction coefficients
β_{ss}, β_{sv}, β_{vs}, β_{vv} phenomenological parameters in chemo-mechanical constitutive laws
Γ_i partial coefficient of ith ion
γ_w water unit weight ($=\rho_w \boldsymbol{g}$)
ε scalar strain in unidimensional geometry
$\boldsymbol{\varepsilon}$ strain tensor
μ_i chemical potential of ith ion in equilibrium bulk solution
$\bar{\mu}_i$ chemical potential of ith ion in pore solution
μ_i^0, $\bar{\mu}_i^0$, μ_w^0, $\bar{\mu}_w^0$ integration constants
μ_i^{ec} electrochemical potential of ith ion in equilibrium bulk solution
$\bar{\mu}_i^{ec}$ electrochemical potential of ith ion in pore solution
μ_k chemical potential of kth fluid component in equilibrium bulk solution
$\bar{\mu}_k$ chemical potential of kth fluid component in pore solution
μ_s salt chemical potential in equilibrium bulk solution
μ_w water chemical potential in equilibrium bulk solution
$\bar{\mu}_w$ water chemical potential in pore solution
ν_i stoichiometric coefficient of ith ion
Π osmotic pressure in equilibrium bulk solution
$\Delta\Pi$ osmotic pressure difference
$\bar{\Pi}$ osmotic pressure in pore solution
Π_b osmotic pressure at bottom boundary of specimen
Π_t osmotic pressure at top boundary of specimen
ρ_w water density
σ scalar total stress in unidimensional geometry
σ' scalar effective stress in unidimensional geometry
$\boldsymbol{\sigma}$ total stress tensor
τ_m matrix tortuosity factor
τ_r restrictive tortuosity factor
ϕ electric potential in equilibrium bulk solution
$\bar{\phi}$ electric potential in pore solution
$\bar{\psi}$ Donnan's electric potential
ω reflection coefficient
ω_g global reflection coefficient
ϖ swelling pressure coefficient

Indexes

i index for ions (1 = cation, 2 = anion)
j index for ions (1 = cation, 2 = anion)
k index for fluid components (w = water, 1 = cation, 2 = anion)

Subscripts

1 cation
2 anion
b bottom of specimen
g global value
sk solid skeleton
t top of specimen
w water

REFERENCES

Auclair, B., Nikonenko, V., Larchet, C., Métayer, M. & Dammak, L. (2002). Correlation between transport parameters of ion-exchange membranes. *J. Membrane Sci*. **195**, No. 1, 89–102.

Coussy, O. (2004). *Poromechanics*. Chichester, UK: Wiley.

Di Emidio, G. (2010). *Hydraulic and chemico-osmotic performance of polymer treated clays*. PhD thesis, Ghent University, Belguim.

Dominijanni, A. & Manassero, M. (2010). Chemico-osmosis and solute transport through geosynthetic clay liners. In *Geosynthetic clay liners for waste containment* (eds A. Bouazza and J. J. Bowders), pp. 105–125. Leiden, the Netherlands: CRC Press.

Dominijanni, A. & Manassero, M. (2012a). Modelling the swelling and osmotic properties of clay soils. Part I: The phenomenological approach. *Int. J. Engng Sci*. **51**, February, 32–50.

Dominijanni, A. & Manassero, M. (2012b). Modelling the swelling and osmotic properties of clay soils. Part II: The physical approach. *Int. J. Engng Sci*. **51**, February, 51–73.

Donnan, F. G. (1911). Theorie der Membrangleichgewichte und Membranpotentiale bei Vorhandensein von nicht dialysierenden Elektrolyten. Ein Beitrag zur physikalisch-chemischen Physiologie [Theory of membrane equilibria and membrane potentials in the presence of non-dialysing electrolytes. A contribution to

physical-chemical physiology]. *Z. Elektrochem. Angew. Phys. Chem*. **17**, No. 14, 572–581. English translation republished 1995 in *J. Membrane Sci*. **100**, No. 1, 45–55.

Dormieux, L., Barboux, P., Coussy, O. & Dangla, P. (1995). A macroscopic model of the swelling phenomenon of a saturated clay. *Eur. J. Mech. A Solids* **14**, No. 6, 981–1004.

Dormieux, L., Lemarchand, E. & Coussy, O. (2003). Macroscopic and micromechanical approaches to the modelling of the osmotic swelling in clays. *Transp. Porous Media* **50**, No. 1, 75–91.

Ehlers, W. (2002). Foundations of multiphasic and porous materials. In *Porous media: Theory, experiments and numerical applications* (eds W. Ehlers and J. Bluhm), pp. 3–86. Berlin, Germany: Springer-Verlag.

Kang, J.-B. & Shackelford, C. D. (2009). Clay membrane testing using a flexible-wall cell under closed-system boundary conditions. *Appl. Clay Sci*. **44**, No. 1–2, 43–58.

Katchalsky, A. & Curran, P. F. (1965). *Nonequilibrium thermodynamics in biophysics*. Cambridge, MA, USA: Harvard University Press.

Kemper, W. D. & Rollins, J. B. (1966). Osmotic efficiency coefficients across compacted clays. *Soil Sci. Soc. Am. J.* **30**, No. 5, 529–534.

Malusis, M. A., Shackelford, C. D. & Olsen, H. W. (2001). A laboratory apparatus to measure chemico-osmotic efficiency coefficients for clay soils. *Geotech. Test. J.* **24**, No. 3, 229–242.

Malusis, M. A. & Shackelford, C. D. (2002a). Chemico-osmotic efficiency of a geosynthetic clay liner. *J. Geotech. Geoenviron. Engng* **128**, No. 2, 97–106.

Malusis, M. A. & Shackelford, C. D. (2002b). Coupling effects during steady-state solute diffusion through a semipermeable clay membrane. *Environ. Sci. Technol*. **36**, No. 6, 1312–1319.

Malusis, M. A., Shackelford, C. D. & Olsen, H. W. (2003). Flow and transport through clay membrane barriers. *Engng Geol*. **70**, No. 3–4, 235–248.

Malusis, M. A., Shackelford, C. D. & Maneval, J. E. (2012). Critical review of coupled flux formulations for clay membranes based on nonequilibrium thermodynamics. *J. Contam. Hydrol*. **138–139**, 40–59.

Manassero, M. & Dominijanni, A. (2003). Modelling the osmosis effect on solute migration through porous media. *Géotechnique* **53**, No. 5, 481–492, http://dx.doi.org/10.1680/geot.2003.53.5.481.

Shackelford, C. D. & Daniel, D. E. (1991). Diffusion in saturated soil: I. Background. *J. Geotech. Engng* **117**, No. 3, 467–484.

Shackelford, C. D., Malusis, M. A. & Olsen, H. W. (2003). Clay membrane behavior for geoenvironmental containment. In *Soil and Rock America Conference 2003* (*Proc. Joint 12th Panamerican Conf. Soil Mech. Geotech. Engng and 39th US Rock Mech. Symp*.) (eds P. J. Culligan, H. H. Einstein and A. J. Whittle), Vol. 1, pp. 767–774. Essen, Germany: Verlag Glückauf GmbH.

Shackelford, C. D. & Lee, J.-M. (2003). The destructive role of diffusion on clay membrane behavior. *Clays Clay Miner*. **51**, No. 2, 186–196.

Yaroshchuk, A. E. (1995). Osmosis and reverse osmosis in fine-charged diaphragms and membranes. *Adv. Colloid Interface Sci*. **60**, No. 1–2, 1–93.

Yeo, S.-S., Shackelford, C. D. & Evans, J. C. (2005). Membrane behaviour of model soil-bentonite backfill mixtures. *J. Geotech. Geoenviron. Engng* **131**, No. 4, 418–429.